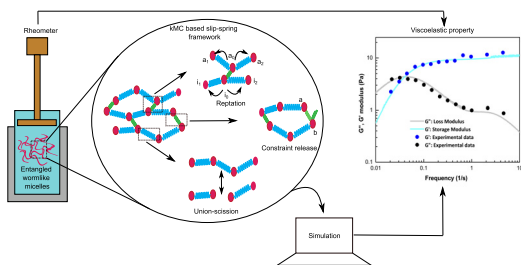


## Regular Article

## A slip-spring framework to study relaxation dynamics of entangled wormlike micelles with kinetic Monte Carlo algorithm

Silabrata Pahari <sup>a,b</sup>, Bhavana Bhadriraju <sup>a,b</sup>, Mustafa Akbulut <sup>a</sup>, Joseph Sang-II Kwon <sup>a,b,\*</sup><sup>a</sup> Artie McFerrin Department of Chemical Engineering, Texas A&M University, College Station, TX 77845, USA<sup>b</sup> Texas A&M Energy Institute, Texas A&M University, College Station, TX 77845, USA

## GRAPHICAL ABSTRACT



## ARTICLE INFO

## Article history:

Received 10 February 2021

Revised 21 April 2021

Accepted 6 May 2021

Available online 11 May 2021

## Keywords:

Wormlike micelles  
Slip-spring framework  
Kinetic Monte Carlo  
Relaxation dynamics  
Linear rheology

## ABSTRACT

**Hypothesis:** Wormlike micelles (WLMs) formed due to the self-assembly of amphiphiles in aqueous solution have similar viscoelastic properties as polymers. Owing to this similarity, in this work, it is postulated that kinetic Monte Carlo (kMC) sampling of slip-springs dynamics, which is able to model the rheology of polymers, can also be extended to capture the relaxation dynamics of WLMs.

**Theory:** The proposed modeling framework considers the following relaxation mechanisms: reptation, union-scission, and constraint release. Specifically, each of these relaxation mechanisms is simulated as separate kMC events that capture the relaxation dynamics while considering the living nature of WLMs within the slip-spring framework. As a case study, the model is implemented to a system of sodium oleate and sodium chloride to predict the linear rheology and the characteristic relaxation times associated with the individual relaxation mechanisms at different pH and salt concentrations.

**Findings:** Linear rheology predictions were found to be in good agreement with experimental data. Furthermore, the calculated relaxation times highlighted that reptation contributed to a continuous increase in viscosity while union-scission contributed to the decrease in viscosity of WLM solutions at a higher salinity and pH. This manifests the proposed model's capability to provide insights into the key processes governing WLM's rheology.

© 2021 Elsevier Inc. All rights reserved.

## 1. Introduction

When amphiphilic surfactant molecules are kept in a polar solvent, the hydrophobic tails of these molecules aggregate together

to form self-assembled supermolecular structures [1–4]. One such supermolecular structure is wormlike micelle (WLM) [5,6]. These WLMs have unique viscoelastic properties which are of interest to numerous industry sectors [7,8]. It has long been noted that WLMs bear many similarities with polymers [9–11], and thus, existing modeling approaches of polymers have been utilized to explain the viscoelastic properties of WLMs. For example,

\* Corresponding author at: Artie McFerrin Department of Chemical Engineering, Texas A&M University, College Station, TX 77845, USA.

E-mail address: [kwon075@tamu.edu](mailto:kwon075@tamu.edu) (J.S.-I. Kwon).

entanglement relaxation dynamics in polymers have been modeled with the reptation-tube-based framework proposed by Edward et al. [12], where the motion of polymers in the entangled state is described by the motion of a single polymer confined in a tube. Then, for the first time, Cates and co-workers extended this reptation-tube-based framework to model relaxation dynamics of WLMs [11]. The major difference between conventional polymers and WLMs, which is the presence of continuous breakage and recombination (i.e., dynamic union-scission), was explicitly considered in Cates' model through breaking the WLM segments with an equal probability and recombining them with probability proportional to the product of the number density of the recombining species. Inspired by the success of Cates' model to explain the relaxation dynamics of WLMs, a few studies have further extended this framework to incorporate more accurate description of the system's rheology [13–15]. Since these studies are based on the reptation-tube theory [12,16,17], it is assumed that the motion of these macromolecules is confined by a tube. However, in practice, owing to the motion of neighboring molecules, the confined space dynamically evolves with time resulting in alterations of entanglements associated with the confined macromolecule, and this phenomenon is termed as constraint release [18,19].

To consider the phenomenon of constraint release in polymers, the slip-link models were proposed in the field of polymer physics, where entanglements are represented by spatially mobile or fixed slip-links [20–22]. These slip-links impose constraints analogous to a confining tube (Fig. A1). However, the conventional slip-link models implemented to study the relaxation of polymer melts were unable to capture the dynamics between entanglements. This limitation was addressed by a modified slip-link model proposed by Likthman, which is referred to as the slip-spring model [23], where the polymer chain was confined by slip-springs anchored to spatially fixed points. This framework was implemented to study the relaxation of a single polymer chain and made excellent predictions of linear rheology. However, the Likthman's slip-spring framework did not consider multi-chain dynamics.

To address the challenges of the Likthman's single chain slip-spring model, Uneyama and Masubuchi [24] combined Likthman's slip-spring framework with Masubuchi's slip-link based multi-chain model [25] by replacing slip-links with slip-springs. The use of slip-springs introduced local pairwise topological constraints that considered the interactions between entangled polymers during multi-chain dynamics. Furthermore, Muller and Dolous [26] investigated the application of the Monte Carlo (MC) algorithm to study the dynamics of slip-spring hopping in polymers. The MC algorithm allowed slip-springs to hop and get created-destroyed. The hopping of slip-springs mimics the relaxation mechanism of reptation, which is analogous to the slithering-snake motion of the polymers, while the creation-destruction of slip-springs captures the process of constraint release. Motivated by these findings, Chappa et al. [27] implemented the MC algorithm to the multi-chain network to compute the configuration of slip-springs along the length of polymers. However, in their work, no kinetics was associated with the MC algorithm, and thus, it was challenging to incorporate the time scale for slip-spring hopping in this model. These challenges were addressed by Vogiatzis et al. [28] via a kinetic Monte Carlo (kMC) scheme. The application of this kMC scheme allowed the model to track the discrete transition in slip-springs with time. Though this approach is suitable for polymer systems, it cannot be directly extended to model the relaxation dynamics of more complex systems like WLMs.

Motivated by the above considerations, in this work, a coarse-grained kMC model for predicting the linear rheology of WLMs at long time scales is developed. In this proposed model, the dynamic union-scission of WLMs is considered as a separate kMC event, and

integrated with the time scale of slip-spring hopping. Additionally, important kinetics like the diffusion-controlled union of WLMs, which is precluded in the Cates model, has also been considered for accurate predictions of dynamic system properties. To our knowledge, the proposed model is the application of the multi-chain slip-spring framework, for the first time, to model the relaxation dynamics of living macromolecular systems like WLMs. To predict the rheological properties of WLMs, the proposed kMC simulation requires the dimensions of WLMs as initial conditions, which can be derived from a thermodynamic model proposed by Danov et al. [29]. Specifically, integrating the thermodynamic model with the proposed kMC model allows to quantitatively describe the change in zero shear viscosity with salt concentration. The effect of pH on the evolution of viscoelasticity as well as on the morphology of WLMs is also explained by the proposed kMC model.

This article is organized as follows: In the model formulation section, the proposed kMC model for rheology prediction is presented. In the simulation methodology section, a detailed implementation of the proposed framework is discussed. In the result section, the major findings from the developed framework are presented. In the conclusion section, a number of significant insights inferred from the simulation results are highlighted.

## 2. Model formulation

In this section, the rheology model necessary for predicting the relaxation dynamics of WLMs has been mathematically formulated. The initial length of WLMs to be used in the rheology model is calculated from a thermodynamic model proposed by Danov et al. [29,30]. Additionally, this section highlights the essential novelty of the present work, which is to develop a coarse-grained slip-spring framework to model the WLM relaxation dynamics via kMC simulations. Details of the developed framework and the important kMC events are explained in the following subsections.

### 2.1. WLM network

The WLM macromolecular chains utilized in modeling rheology are created by following a two-step procedure. Firstly, chains composed of freely jointed Khun's segments are created. In these chains, individual Khun's segments bear no directional correlation with the others. Following the generation of these freely jointed chains, coarse-graining is performed by aggregating a certain number of Khun's segments and replacing them with beads. These beads are then inter-connected by entropic springs. In the produced system of WLMs, each bead  $i$  located along the contour of WLMs has a three dimensional position vector,  $r_i$ , and represents a collection of multiple Khun's segments.

The WLM network considered here is illustrated in Fig. 1, where the entanglements are represented by entropic slip-springs that impose topological constraints. In this work, first, the slip-springs can hop along the contour length from one bead to another following a kMC algorithm, which mimics reptation in WLMs. Second, constraint release in the collection of WLMs is also simulated by considering the creation and destruction of slip-springs in the kMC algorithm. Third, the kMC simulation explicitly takes into account the union-scission process of WLMs. To account for the stochastic forces acting on the WLMs due to solvent molecules, Brownian Dynamics (BD) simulations of WLMs is performed in parallel with the kMC simulation in a periodic simulation box. An overview of implementing the BD and kMC algorithm to the slip-spring framework is illustrated in Fig. A2. In the remaining portion of this section, each step of the proposed rheology model is detailed.

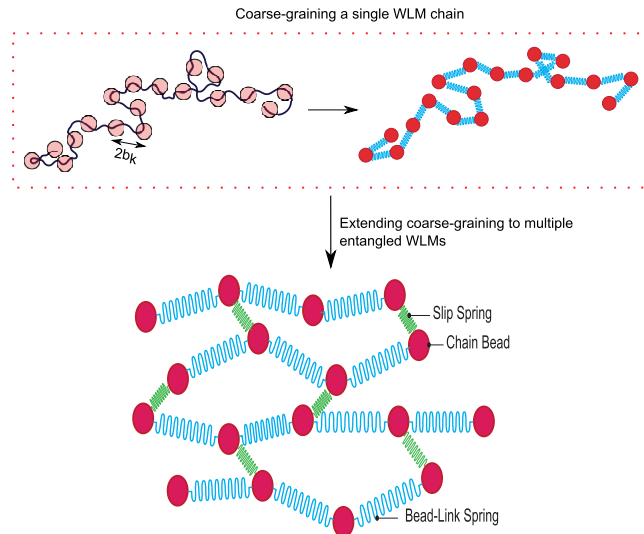


**Fig. 1.** Coarse-graining methodology and the representation of entangled WLM network with slip-springs.

### 2.1.1. Modeling potential energy

In this section, the bonding and non-bonding forces required to model the relaxation dynamics in WLMs are calculated. The entanglement dynamics of the WLM melt is governed by Helmholtz free energy. The total Helmholtz free energy of WLM melts is obtained as follows:

$$A_{\text{total}} = A_{\text{bonded}}(r_{ij}, T) + A_{\text{non-bonded}}(\rho(r), T) \quad (1)$$

where  $A_{\text{bonded}}(r_{ij}, T)$  is the bonded energy,  $r_{ij}$  is the pairwise distance between bead  $i$  and bead  $j$  connected through a spring or a slip-spring. Specifically,  $A_{\text{bonded}}(r_{ij}, T)$  is given as follows:

$$A_{\text{bonded}}(r_{ij}, T) = \sum_{j=1}^{N_{\text{springs}}} \frac{3k_b T (r_i - r_j)^2}{2N_s b^2} + \sum_{j=1}^{N_{\text{slip-springs}}} \frac{3k_b T (r_i - r_j)^2}{2K_{ss}^2} \quad (2)$$

where  $b$  is the Khun's length,  $r_i$  and  $r_j$  are the position vectors from the origin to bead  $i$  and bead  $j$ , respectively,  $N_s$  is the number of Khun's segments between the bonded springs,  $K_{ss}$  is the slip-spring stiffness constant,  $T$  is the temperature of WLM melt, and  $k_b$  is the Boltzmann constant. The bonding force acting on bead  $i$  due to connection with bead  $j$ ,  $F_{ij}^b$ , is given by the gradient of bonding potential associated with bead  $i$  as follows:

$$F_{ij}^b = -\nabla A_{\text{bonded}}(r_{ij}, T) \quad (3)$$

The non-bonding interaction between the beads accounts for the excluded-volume interactions along with the Van der Waals attractive forces. To evaluate the non-bonding interactions, the Helmholtz potential due to non-bonded interaction is given as follows:

$$A_{\text{non-bonded}} = \oint a_{\text{vol}}[(\rho(r), T)] dr_1 dr_2 dr_3 \quad (4)$$

where  $a_{\text{vol}}[(\rho(r), T)]$  is the Helmholtz potential due to non-bonding interaction per unit volume, and  $\rho(r)$  is the local mass density of WLM melts. To evaluate  $a_{\text{vol}}[\rho(r), T]$ , Sanchez Lacombe equation of state is used as mentioned below [31]:

$$a_{\text{vol}}(\rho(r), T) = \rho_{\text{mass}} a_{\text{mass}}(\rho(r), T) \quad (5)$$

$$a_{\text{mass}}(\rho, T) = \frac{-rRT^* \hat{\rho}}{(\rho^*)^2} \rho + \frac{p^* \hat{T}}{\rho^*} \left[ \left( \frac{\rho^*}{\rho} - 1 \right) \ln \left( 1 - \frac{\rho}{\rho^*} \right) + \frac{RT \rho^*}{Mp^*} \ln \left( \frac{\rho}{w \rho^*} \right) \right] \quad (6)$$

$$r = \frac{Mp^*}{RT \rho^*} \quad (7)$$

where  $\rho^*$  is the critical density of WLM melts,  $T^*$  is the critical temperature of WLM melts,  $p^*$  is the critical pressure of WLM melts,  $w$  is the parameter quantifying the number of configurations of the system available,  $a_{\text{mass}}(\rho(r), T)$  is the Helmholtz potential due to non-bonding interaction per unit mass,  $\hat{\rho} = \frac{\rho}{\rho^*}$  is the reduced density of WLM melts,  $\hat{T}$  is the reduced temperature,  $R$  is the universal gas constant,  $M$  is the molecular weight of WLM chains, and  $r$  is the number of Sanchez Lacombe segments assumed to be constituting WLM chains. The obtained value of Helmholtz potential due to non-bonding interactions is used to calculate the non-bonding force by taking the gradient of the derived potential as follows:

$$F_i^{\text{nb}} = -\nabla_{r_i} A_{\text{nb}}(\rho_{\text{cell}}, T) = -\sum_{i=1}^{N_{\text{cells}}} \frac{\partial(a_{\text{vol}}(\rho, T))}{\partial \rho} \frac{\partial(\rho_{\text{cell},k})}{\partial r_i} \quad (8)$$

$$\frac{\partial a_{\text{vol}}(\rho, T)}{\partial \rho} = \frac{-2p^*}{(\rho^*)^2} \rho - \frac{p^* T}{\rho^* T} \left[ 1 + \ln \left( 1 - \frac{\rho}{\rho^*} \right) \right] + \frac{RT}{M} \left[ 1 + \ln \left( \frac{\rho}{\rho^* w} \right) \right] \quad (9)$$

As the next step, the obtained bonding and non-bonding forces are used in the BD simulations.

### 2.1.2. Brownian dynamics

The effect of solvent molecules on the beads of WLM melts is captured by utilizing BD simulations, which are useful in continuously updating the position of beads in chains via Langevin equation. For this purpose, the Langevin equation is integrated with the method of Gunsteren and Berendsen as follows [32]:

$$r_i(t + \delta t) = r_i(t) + \frac{1}{\zeta_i} \left[ F_i(t) \delta t + \frac{1}{2} F_i(t) (\delta t)^2 \right] + G_i(t) \quad (10)$$

$$F_i(t) = -\nabla_{r_i} (A_{\text{bonded}}(r_{ij}, T) + A_{\text{non-bonded}}[\rho(r, t)]) \quad (11)$$

$$F_i(t) = \frac{F_i(t) - F_i(t - \delta t)}{\delta t} \quad (12)$$

$$G_i(t) = N \left( 0, \frac{2k_b T \delta t}{\zeta_i} \right) \quad (13)$$

where  $G_i(t)$  is white Gaussian noise,  $\delta t$  is the integration time-step in the BD simulation, and  $\zeta_i$  is the friction coefficient of the solution. In the above equations, the approximation of the time derivative of force is done using the finite difference method. The bonding and non-bonding forces calculated from the previous section are utilized in Eq. (11). The updated position vectors obtained from the BD simulation are used in the subsequent kMC events executed to capture different relaxation mechanisms in WLM chains.

### 2.1.3. kMC for slip-spring hopping

The kMC step allocates the hopping of slip-springs from one bead to another to mimic the reptation phenomenon. Whenever a slip-spring hops from one bead at a particular energy state to another, it goes through a transition state. Inside the chain, as all the beads except for the end-beads are alike, it is assumed that the transition energy for all the hops within the internal beads is similar. This assumption was done for a similar system involving the simulation of the relaxation dynamics of the long chain polymers by Vogiatzis et al. [28]. Because of this assumption, the rate of hopping depends only on the initial state or energy of the slip-spring. Accordingly, activation energy for the slip-spring hopping is obtained as follows:

$$A_{\text{activation}} = A_{\text{transition}}^* - A_0 \quad (14)$$

where  $A_0$  is the initial state before the activation of slip-spring,  $A_{\text{transition}}^*$  is the transition energy, and  $A_{\text{activation}}$  is the activation energy associated with a slip-spring to move from an initial state to an activated state. Further, the rate of hopping is given by an Arrhenius type equation using the activation energy obtained from Eq. (14) as follows:

$$r_{hopping} = v_{hop} \exp\left(\frac{-A_{activation}}{k_b T}\right) \\ = \underbrace{v_{hop} \exp\left(\frac{-A_{transition}^*}{k_b T}\right)}_{K_{hop}} \exp\left(\frac{A_0}{k_b T}\right) \quad (15)$$

where  $v_{hop}$  is the rate constant, and  $K_{hop}$  is the combined rate constant. Since the activation energy for a slip-spring to hop from one bead to another bead is the same for all internal beads, the term  $\exp\left(\frac{-A_{transition}^*}{k_b T}\right)$  remains constant, and hence, can be combined with  $v_{hop}$  (as a single parameter  $K_{hop}$ ). An illustration of the hopping event is presented in Fig. 2a.

#### 2.1.4. kMC for slip-spring creation-destruction and constraint release

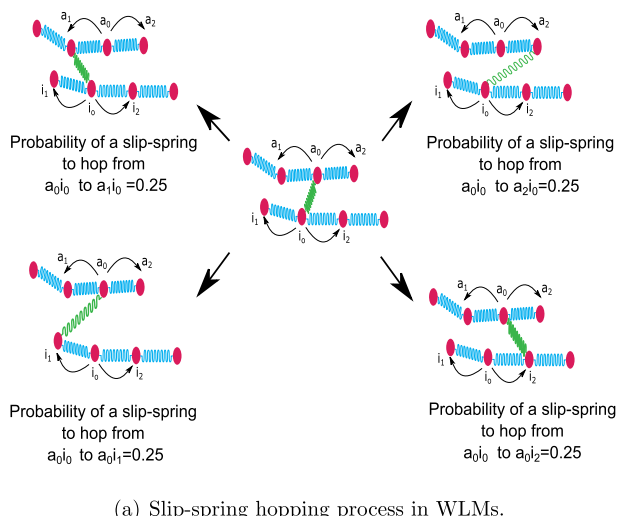
When a slip-spring reaches the end-bead of a WLM chain through the slip-spring hopping process, it may hop out from the last bead. Once the slip-spring hops out, it gets destroyed, and in turn, a new slip-spring gets created in the WLM melt. The process of slip-spring creation and destruction is highlighted in Fig. 2b. Note that the length of slip-spring that gets created at a new location should be within proper bounds. Moreover, in this work, the number of slip-springs is kept constant, and therefore, whenever the slip-spring destruction takes place in WLM melts, a new slip-spring is simultaneously created. Thus, the probability for slip-spring destruction at the chain end is associated with the formation of slip-spring somewhere else in WLM melts, which is referred to as the slip-spring destruction-creation event while the reverse

of this event is the creation-destruction event. The probabilities of these processes are evaluated by utilizing the Rosenbluth weight function [33], defined as  $W = \sum_{j=1}^{N_{radius}} \exp\left(-\frac{A_{a,b_j}}{k_b T}\right)$ , as follows:

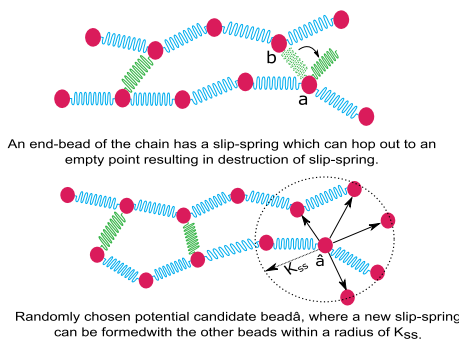
$$P_{(creation-destruction)} = \frac{\exp\left(-\frac{A_{a,b}}{k_b T}\right)}{W_N} P_{ss} \quad (16)$$

$$P_{(destruction-creation)} = \frac{\exp\left(-\frac{A_{a,b}}{k_b T}\right)}{W_O} P'_{ss} \quad (17)$$

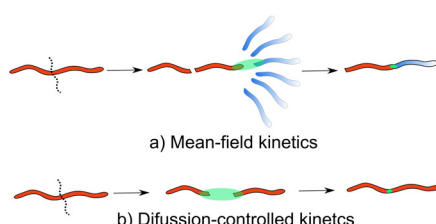
where  $N_{radius}$  represents the number of possible slip-springs that are within a radius of  $K_{ss}$  from a candidate bead at which a slip-spring may get created,  $(a, b)$  is the old location of the destroyed slip-spring (which is the chain end),  $(\hat{a}, \hat{b})$  is the location of the newly created slip-spring,  $W_O$  and  $W_N$  are the Rosenbluth weight functions for the old and new configurations, respectively,  $P_{ss}$  is the probability of accepting the move of destruction-creation, and  $P'_{ss}$  is the probability of accepting the move of creation-destruction. Note that the events of creation-destruction and destruction-creation of slips-springs are reversible in nature. This condition of reversibility implies that the probability of destruction-creation (i.e., the probability of a slip-spring to get destroyed at a location  $(a, b)$  and formed at a new location  $(\hat{a}, \hat{b})$ ) is equal to the probability of creation-destruction (i.e., the probability for the slip-spring formed at  $(\hat{a}, \hat{b})$  to get destroyed and formed at  $(a, b)$ ). Applying this



(a) Slip-spring hopping process in WLMs.



(b) Creation-destruction event of slip-springs in WLMs .



(c) Union-scission in WLMs .

Fig. 2. Illustration of different relaxation mechanisms in WLMs considered in the proposed framework.

criterion of reversibility to Eqs. 16,17, the values for  $P_{ss}$  and  $P'_{ss}$  are obtained as follows:

$$P_{ss} = \min \left[ 1, \exp \left( -\frac{A_{\dot{a},\dot{b}} - A_{a,b}}{k_b T} \right) \frac{W_N}{W_O} \right] \quad (18)$$

$$P'_{ss} = \min \left[ 1, \exp \left( -\frac{A_{a,b} - A_{\dot{a},\dot{b}}}{k_b T} \right) \frac{W_O}{W_N} \right] \quad (19)$$

This dynamic creation and destruction of slip-springs in WLM melts captures the phenomenon of constraint release.

### 2.1.5. kMC for union-scission in WLMs

The union-scission process in WLMs follows two classes of kinetics which are the mean-field kinetics [11] and diffusion-controlled kinetics [34]. In the mean-field kinetics, WLMs break and diffuse to recombine with other segments, instead of the ones created from the same parent WLM. On the other hand, in the case of diffusion-controlled kinetics, the WLMs recombine with the segment created from the same parent to produce the original WLM. An illustration of these two kinetics is highlighted in Fig. 2c. In this work, the process of dynamic union-scission is executed with a kMC step wherein two events are considered. The first event considered is the WLM breakage where each segment of the WLM chain has an equal probability of breakage. The second event considered is the recombination of WLMs where the rate is proportional to the product of the concentrations of WLM segments recombining to form new WLM chains. The time-scale for recombination and breakage in WLMs is of the same order, and is denoted as  $t_{break}$ . The time taken for the WLMs to diffuse to the nearest endcaps for recombination is given by  $t_h$ . When  $t_{break} > t_h$  (i.e., the time taken by the WLMs to recombine is longer than the time taken for the WLMs to diffuse to the nearest endcaps), the mean-field kinetics holds true. Conversely, when  $t_{break} < t_h$ , recombination occurs and diffusion-controlled kinetics, takes place. In the diffusion-controlled regime, multiple breakage and self-recombination occur in the span of one diffusion time,  $t_h$ . On the contrary, once the diffusion time passes (i.e.,  $t > t_h$ ), the WLMs migrate to the nearest endcaps and recombine. The corresponding rates for the recombination and breakage of WLMs are given as follows:

$$r_{breakage} = 2k_{break}N_s \quad (20)$$

$$r_{recombination} = k_{break}\exp(-N_s b) \quad (21)$$

where  $k_{break}$  is the rate constant for breakage reaction in WLMs. The linearity in Eq. 20 arises because each Kuhn's segment forming the WLM chain has an equal probability of breakage. Hence, the probability of breakage increases linearly as more Kuhn's segments are required to form longer WLM chains [10,11]. Furthermore, owing to the microscopic reversibility criterion of Kuhn's segments, there is a decreasing propensity of WLM chains to recombine as their length increases. Subsequently, a physical interpretation of these rate equations [i.e., Eq. (20) and (21)] is that once the WLM system has longer chains, it loses the driving force to recombine with others and instead prefers to break into smaller chains.

## 3. Model implementation

In this section, the implementation of the proposed kMC model is discussed. Also, a brief overview of the thermodynamic model utilized to calculate the initial length of WLMs for rheology modeling is presented in Appendix B.

### 3.1. Proposed rheology model simulation

The values of the parameters used for simulations are highlighted in Appendix E. The simulation domain is a three-dimensional periodic box with dimensions of  $10^3 \times 10^3 \times 10^3$  nm<sup>3</sup>. The Kuhn's length,  $b$ , is obtained from the persistence length,  $l_p$ , as  $b = 2l_p$ . Once the Kuhn's length is attained, freely jointed WLM chains are generated with the Kuhn's segments. These generated WLM chains are subject to a Monte Carlo (MC) simulation to obtain the initial configuration of WLMs at which the density and free energy of the WLM melt has minimum fluctuations [35]. Following the MC simulations, coarse-graining of the WLM melt is done by aggregating four Kuhn's segments per unit bead. After obtaining the coarse-grained WLM melts, slip-springs are added to the system. The number of slip-springs is in accordance with the entanglement length,  $l_e$ , of WLMs. Furthermore, owing to their long length, WLMs can be approximated by the loosely entangled regimes as pointed out by Zou et al. [36]. The value of  $l_e$  is calculated from the persistence length as  $l_e = \frac{N_k b^2}{2l_p}$ , and the number of slip-springs/entanglements is calculated as  $\langle Z \rangle = \frac{\langle l \rangle}{l_e}$  [36]. The entanglement stiffness constant,  $K_{ss}$ , is a parameter that is determined from fitting the experimental data with the model predictions. The value of  $K_{ss}$  is 70.4 nm, and it satisfies the condition  $K_{ss} > \sqrt{N_k}b$ , thus making the slip-springs less stiff than the harmonic springs connecting the WLM beads.

In the BD simulation, the force due to the solvent molecules acting on the WLM beads is modeled via the solvent friction coefficient,  $\zeta_i$ , which characterizes the resistance encountered by a bead moving through the solvent, and its value is presented in Appendix E.

The hopping rate constant is calculated as  $K_{hop} = \mu \frac{N_{ss}}{N_{beads}}$ , where  $N_{ss}$  is the total number of slip-springs present in the WLM melt,  $N_{beads}$  is the total number of beads in the system, and the value of the constant  $\mu$  is mentioned in Appendix E. The time increment for the slip-spring hopping and constraint-release is identical, and the corresponding time for these events is obtained as  $\delta t_{rep} = N_{kMC} dt$ , where  $N_{kMC}$  is the number of BD steps integrated per unit slip-spring transition step. Here,  $\delta t_{rep}$  is the regular time increment after which slip-spring transition is sampled and  $dt = 10^{-9}$  seconds is the time increment for the BD simulation. Thus, after every  $N_{kMC}$  steps of the BD simulation, the coordinates for beads are frozen, and the events of slip-spring hopping and slip-spring creation-destruction are executed.

**Remark 1.** In the event of slip-spring creation, one end of the slip-spring is chosen randomly from the beads present in the WLM melt, while the other end of the slip-spring is chosen from the beads belonging to neighboring WLM chains and lying within the maximum length of slip-spring extension,  $K_{ss}$ . Thus, the maximum extension of all the slip-springs during the creation and destruction is kept within 70.4 nm.

In simulating the union and scission events for WLM relaxation, firstly the class of kinetics is determined by evaluating the breakage time increment [37],  $\Delta t_{break} = k_{b1} < L >$ , and diffusion time increment [37],  $\Delta t_h = k_{b2} < L >^{5/3}$ , where the values of  $k_{b1}$  and  $k_{b2}$  are given in Appendix E. If  $\Delta t_h < \Delta t_{break}$ , mean-field kinetics is selected; otherwise, diffusion-controlled kinetics is selected. The time increment during the union-scission event is  $\delta_t = \frac{\Delta t_{break}}{(2N_{WLMs})}$ , where  $N_{WLMs}$  is the number of WLMs present in the melt. As the breakage time is divided by the number of WLMs present, at every time instant only one breakage or recombination event can take place. In the case of applying the kMC model to mean-field kinetics, either the recombination or breakage events are executed with a

probability of 50% at every time-step. Then, a WLM is chosen randomly and the corresponding event of breakage or recombination is executed with a probability of  $P = \min(1, r_{(breakage/recombination)}\delta_t)$ . However, in the case of diffusion-controlled kinetics ( $\Delta t_h > \Delta t_{break}$ ), at every kMC time step in the interval,  $0 < t < \Delta t_h$ , a series of breakage and self-recombination is executed by sampling a random chain from the WLM melt, and performing the breakage with a probability of  $P = \min(1, r_{breakage}\delta_t)$ . If this corresponding chain is chosen for breakage again within the future time interval of  $0 < t < \Delta t_h$ , the two existing segments are first recombined, and only after that further breakage is performed. At  $t = \Delta t_h$ , the WLMs are allowed to diffuse to the neighboring end-caps and recombine with a probability of  $P = \min(1, r_{recombination}\delta_t)$ . This process is continued until the end of simulation. Fig. A3 illustrates the implementation of diffusion-controlled kinetics. In the BD and kMC simulations, the integration of different time scales and length scales using the proposed framework is highlighted in Fig. A4. While the BD simulations capture the WLM dynamics at the most microscopic level, the kMC event for the union-scission relaxation mechanism captures the system dynamics at the most macroscopic level [42–47]. A snapshot of the BD simulation box with the WLM chains and slip-springs (as used in the computer simulations) is highlighted in the supplementary material (Fig. A5).

#### 4. Results and discussion

The proposed framework is applied to a solution of sodium oleate and sodium chloride which forms WLMs at proper surfactant concentration, salt concentration and pH. The WLMs are sensitive to salt concentration and pH. Therefore, the developed rheology model is utilized to study the effect of salt concentration and pH on the zero shear viscosity of WLMs. In this work, the free energy for the WLMs is obtained from a thermodynamic model proposed by Danov et al. [29]. However, it is to be noted that the thermodynamic model considered in this study is sensitive to the chemical nature of the amphiphiles, and all the model predictions highlighted in this section are explicitly for the CTAB surfactant.

##### 4.1. Thermodynamic model predictions

The WLMs formed due to the self-assembly of amphiphiles tend to minimize the free energy associated with their spherical and cylindrical portions individually. A minimum in free energy due to the WLM formation gives the radius of the cylindrical and spher-

ical portions of these macromolecules. This free energy is further utilized in the thermodynamic model to calculate the initial length of WLMs, which are to be used for dynamic relaxation simulations. Incorporating the length obtained from the thermodynamic model into the rheology model allows the consideration of electrostatic interactions in the relaxation dynamics of WLMs by varying the breakage time and the number of slip-springs (i.e., number of entanglements) associated with a WLM chain.

In Fig. 3a and Fig. 3b, the minimum free energy is achieved at the values of equilibrium radius for the cylindrical and spherical portions of WLMs, respectively. These equilibrium diameters are utilized to predict the mass mean aggregation number from which the mean WLM length is derived by simple geometric considerations that are detailed in Appendix D. Furthermore, Fig. 4 shows the theoretical predictions of the WLM's mean length obtained from the thermodynamic model. Specifically, it highlights the variation of the mean length of WLMs with salt concentration and pH. It can be seen that increasing the salt concentration results in an increase in WLM length due to increased screening by  $\text{Na}^+$  counterions. However, the salt concentration can only be increased up to a particular threshold, beyond which the surfactants start forming a separate phase (known as the salting-out zone), which is not

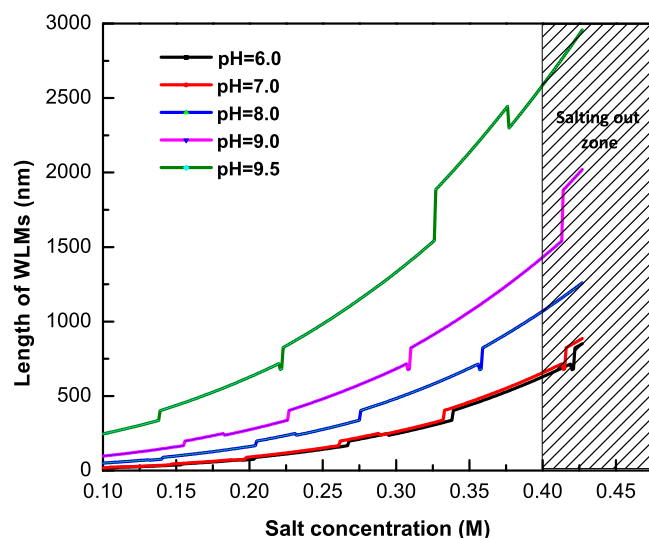


Fig. 4. The effect of salt concentration and pH on the average length of WLMs.

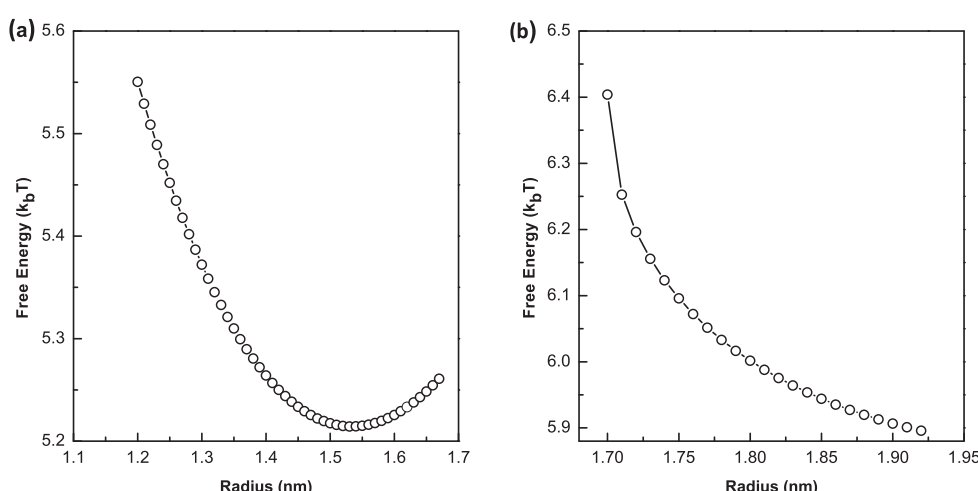
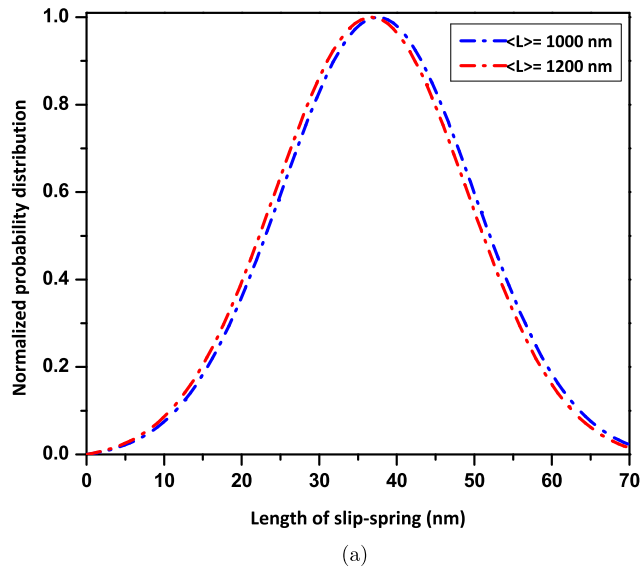
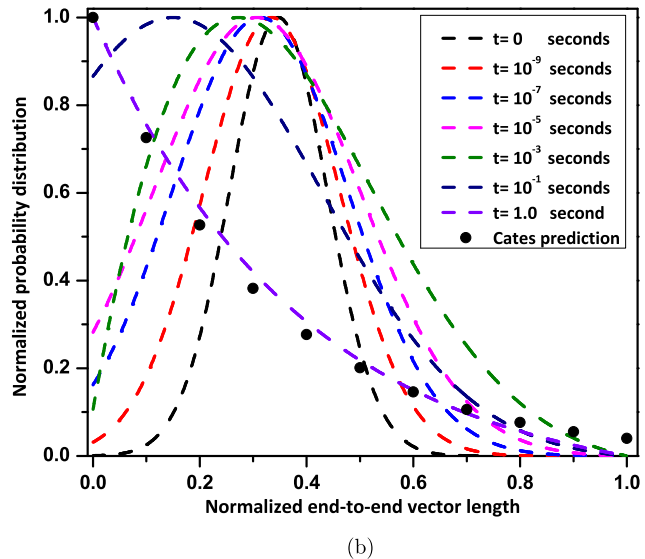


Fig. 3. Free energy plots at  $T = 300$  K for (a) the cylindrical portion of WLMs, and (b) the spherical portion of WLMs.



(a)



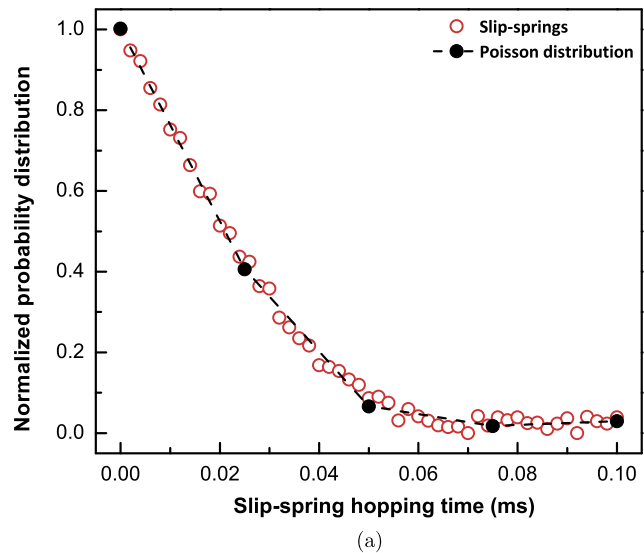
(b)

**Fig. 5.** Illustration of (a) The end-to-end vector length distribution of the slip-springs, and (b) Time evolution of the end-to-end vector length distribution of WLM chains.

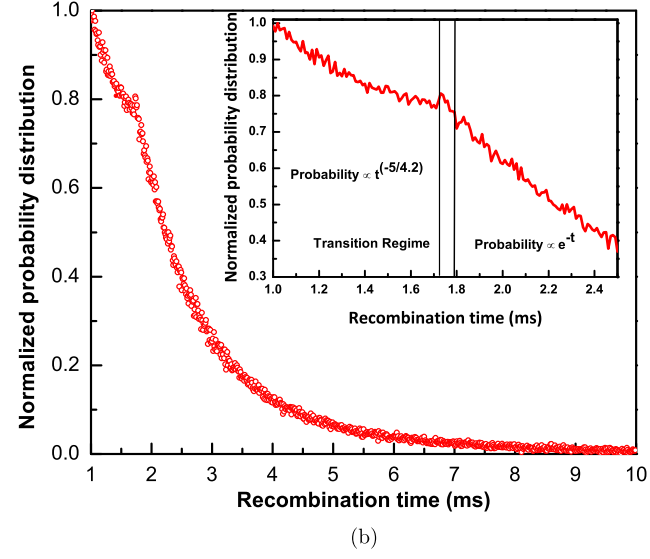
desirable. Furthermore, varying the pH alters the ionic strength of the solution, which impacts the overall electrostatic potential. Consequently, such varying electrostatic potential influences the dimensions of the WLMs. Specifically, increasing the pH through the addition of NaOH increases the number of  $\text{Na}^+$  ions, which in turn increases the ionic strength and the length of WLMs. It is to be noted that the length of WLMs will not be constant due to the dynamic union-scission process. The statistics of WLM length distribution will be discussed in the following section.

#### 4.2. Structural properties of WLM melts

The distribution of the end-to-end vector length of the slip-springs in the simulation domain is highlighted in Fig. 5a. Since the end-to-end vector length of the slip-spring highlights the distance between the WLMs at the entanglement points, analyzing the distribution of the slip-spring length provides a better under-



(a)



(b)

**Fig. 6.** Illustration of (a) Time distribution of the slip-spring hopping in WLMs, and (b) Recombination time distribution from the union-scission of WLMs.

**Table 1**

Comparing the probability distribution of recombination time based on the reptation-tube-based theory and proposed model.

| Time range | Reptation-tube-based theory    | Proposed model                   |
|------------|--------------------------------|----------------------------------|
| $t < t_h$  | Probability $\propto t^{-5/4}$ | Probability $\propto t^{-5/4.2}$ |
| $t > t_h$  | Probability $\propto e^{-t}$   | Probability $\propto e^{-t}$     |

standing of the average distance between the WLMs at these points. Furthermore, it is known that the electric double layer (EDL) of the WLMs extends to a thickness of 0.5 nm from the WLM's surface [29]. Subsequently, to compare the thickness of the EDLs with the distance between the WLM chains, a comparison of the former with the length of the slip-springs could be considered. Hence, from the slip-spring's length distribution illustrated in Fig. 5a it is highlighted that the average distance between the WLMs at the entanglement points is sufficiently large that the EDL attains the asymptotic conditions. The end-to-end vector lengths (i.e., length of the vector that points from one end of a WLM chain to the other end) of WLMs at different times are shown

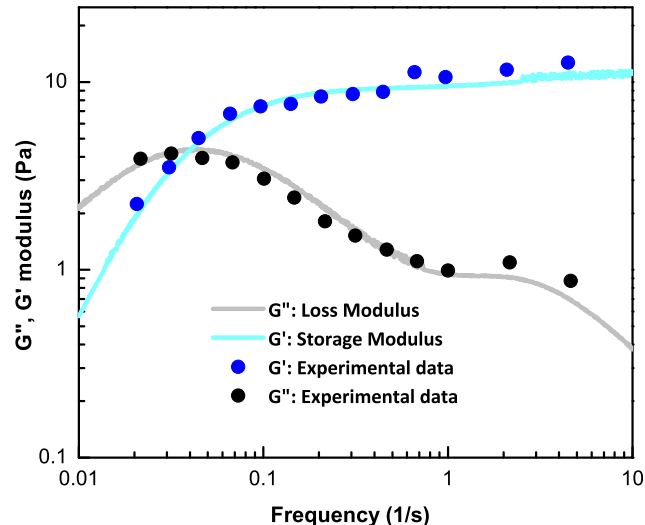


**Fig. 7.** Validation of the model for salt (sodium chloride) concentration of 0.300 M, surfactant (sodium oleate) concentration of 0.065 M, and pH = 9.3.

**Table 2**  
NRMSE with respect to salt concentration.

| Salt concentration | NRMSE |
|--------------------|-------|
| <50 mM             | >0.36 |
| 100 mM             | 0.28  |
| 200 mM             | 0.17  |
| 300 mM             | 0.06  |

in Fig. 5b, which highlights the evolution of the WLM chain length distribution after self-assembly due to dynamic relaxation. It is observed that at shorter times, the end-to-end vector length of WLMs follows a Gaussian distribution. However, the variance of the distribution increases with time, and the Gaussian distribution eventually transitions to an exponential distribution. This transition is a result of the recombination and breakage kinetics, which does not allow the growth of very long chains as these chains tend to quickly break. An important observation is that the computed equilibrium distribution aligns well with the theoretical distribution function predicted by Cates [10] (Fig. 5b). This shows the ability of the coarse-grained chains to replicate the behavior of living polymers like WLMs [38].

#### 4.3. Slip-spring hopping and recombination time distributions

To observe how the reptation phenomenon is captured in the proposed model, analysis of the reptation time is performed. The reptation time distribution, which can be viewed as the slip-spring hopping time distribution obtained from the proposed modeling framework, is shown in Fig. 6a. As slip-spring hopping is a rare event, the hopping times follow a Poisson distribution. To capture the union-scission in WLMs, the recombination times obtained from the proposed model are analyzed for both the kinetic regimes (i.e., mean-field and diffusion-controlled kinetics). Fig. 6b shows that the recombination time distribution for the diffusion-controlled kinetics exhibits a transition in its slope at the diffusion time,  $t_h$ .

This is because the WLMs undergo continuous self-recombination for time  $t < t_h$ . However, for  $t > t_h$ , the WLMs have a sufficient time to migrate to the endcaps of neighboring WLMs and recombine with them, thereby following the mean-field kinetics. For times  $t < t_h$ , the probability distribution function has a slope proportional to  $t^{-5/4,2}$ . This is expected to affect the relaxation dynamics of WLMs at short times. It can also be observed that at long times, there is an exponential decay of the probability distribution function. These results are in accordance with the existing theory of WLM relaxation based on the reptation-tube framework [7,11], presented in Table 1. Hence, it can be inferred that the proposed framework is capable of modeling the dynamics of living systems like WLMs.

#### 4.4. Prediction of storage and loss modulus in WLMs

The primary objective of the developed framework is to predict the linear rheology of WLMs, which is obtained from shear-stress calculations. Relaxation modulus is evaluated at every time step with the help of fluctuation-dissipation theorem as follows:

$$\tau_{\alpha,\beta}(r_{ij}, T) = \frac{1}{V_R} \sum_{i,j}^{N_{\text{segments}}} \frac{\partial A_{\text{bonded}}(r_{ij}, T)}{\partial r_{ij}} \frac{r_{ij,\alpha} r_{ij,\beta}}{r_{ij}} (1 - \delta_{\alpha,\beta}) \quad (22)$$

$$G(t) = \frac{V_R}{k_b T} \langle \tau_{\alpha,\beta}(t_0 + t) \tau_{\alpha,\beta}(t_0) \rangle \quad (23)$$

$$G'(\omega) = \omega \int_0^\infty \sin(\omega t) G(t) dt \quad (24)$$

$$G''(\omega) = \omega \int_0^\infty \cos(\omega t) G(t) dt \quad (25)$$

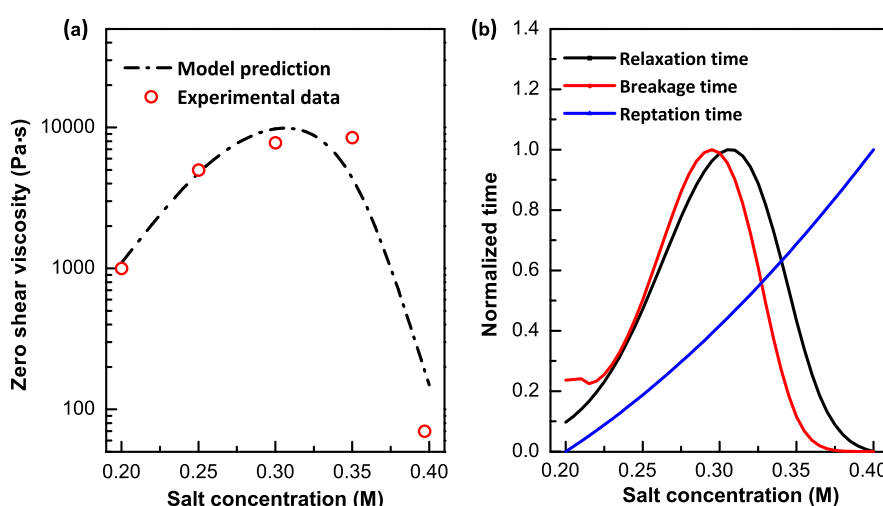


**Fig. 8.** The effect of salt concentration on (a) the zero shear viscosity predicted by the developed model, and (b) the reptation, breakage, and relaxation times.

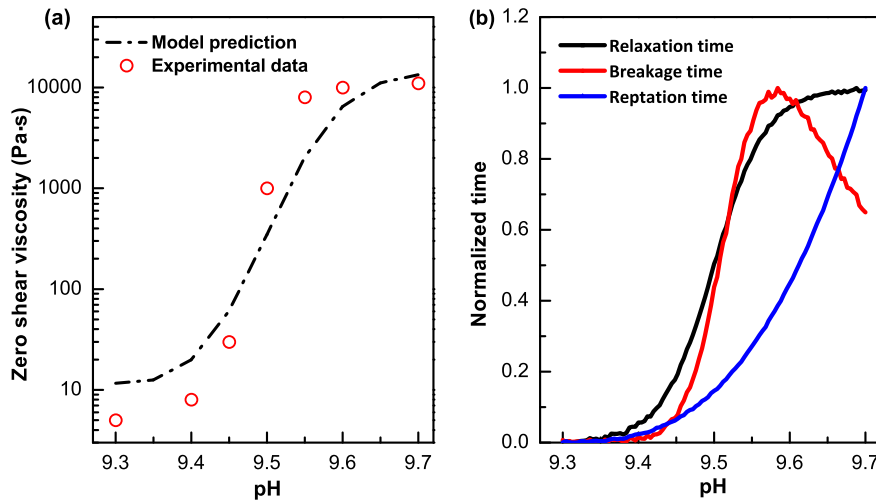


**Fig. 9.** The effect of pH on (a) the zero shear viscosity predicted by the developed model, and (b) the reptation, breakage, and relaxation times.

where  $\alpha$  and  $\beta$  are the orthogonal coordinates of the reference frame,  $V_R$  is the volume of simulation box,  $G(t)$  is the stress relaxation modulus of WLM melts, and  $G'(\omega)$  and  $G''(\omega)$  are the storage and loss modulus of WLM melts, respectively. In particular, the developed model is utilized to predict the storage and loss modulus for different values of salt concentration and pH. The model prediction for the storage modulus and loss modulus is validated with the experimental data [39], and the results are shown in Fig. 7 from which it can be observed that model predictions align well with the experimental data. The crossover frequency obtained from the model predictions is 0.004 Hz, while its value reported in the experimental data is 0.0036 Hz [39]. The normalized root mean squared error (NRMSE) of the model predictions shown in Table 2 highlight that the model does not perform well at a low salt concentration ( $< 0.15$  M) and predicts well at a relatively high salt concentration ( $> 0.20$  M). This is because of the decreasing screening effect with decreasing salt concentration. However, at an extremely high salt concentration (i.e., for values close to 0.40 M), the prediction accuracy of the model decreases due to the undesirable salting-out effect, leading to a high prediction NRMSE.

#### 4.5. Prediction of the zero shear viscosity of solution

After validating the proposed model, it is utilized to capture the variation in the viscosity of solution at extremely low shear rate, with salt concentration and pH. This viscosity at low shear rate is often termed as the solution's zero shear viscosity. The zero shear viscosity is calculated by evaluating the relaxation time, which is the average time taken by a WLM chain to disentangle from all the topological constraints restraining its motion in the WLM melt. The relaxation time,  $\tau_i$ , is obtained by fitting the relaxation modulus to a Maxwell function of the form given by the relation,  $G(t) = \sum_{i=1}^N G_i^0 \exp(-t/\tau_i)$ , where  $\tau_i$  is the relaxation time and  $G_i^0$  is the amplitude of Maxwell's modes [40]. From the relaxation time, the loss modulus is evaluated [Eq. (25)] to calculate the zero shear viscosity via the following equation:

$$\eta = \lim_{\omega \rightarrow 0} \frac{G''(\omega)}{\omega} \quad (26)$$

It can be observed that the zero shear viscosity depends on the relaxation modulus  $G(t)$ , which is a function of the relaxation time. However, the relaxation time is associated with the critical relaxation mechanisms of the WLM melt such as reptation, constraint

release, and union-scission. Thus, the relaxation time depends on the reptation time and breakage time, which are the characteristic times associated with reptation and union-scission, respectively. Hence, an analysis of these times using the proposed kMC model explains the behavior of the relaxation time, which in turn aids in understanding the observed trend in the zero shear viscosity of solution. The predictions of zero shear viscosity with salt concentration and pH are presented in Fig. 8a and Fig. 9a, respectively. It can be seen that the model predictions align well with the experiment data. Furthermore, the dependence of the relaxation time, reptation time, and breakage time on salt concentration and pH is highlighted in Fig. 8b and Fig. 9b. It is evident from these results that both the reptation and breakage times jointly determine the overall trend of the relaxation time, thereby the same in the zero shear viscosity of solution. The major reason for the fall in relaxation time in Fig. 8b and the appreciable fall in its gradient in Fig. 9b is attributed to the fall in breakage times at a high salt concentration and pH, respectively. Since the breakage time is associated with the union-scission mechanism, the variation in zero shear viscosity with salt concentration and pH can be attributed to the living nature of WLMs. On the other hand, increasing salt concentration or pH leads to a continuous rise in the reptation times of WLMs. This is because of the increasing entanglements resulting from the increasing lengths of WLM chains. Hence, the interplay between the reptation and breakage times contribute to the observed sensitivity of the WLM's zero shear viscosity with the salt concentration and pH.

The results and discussions presented in this section provide a few key insights into the linear rheology of WLMs. The major inferences from these results are summarized in the following section.

#### 5. Conclusion

In this work, a kMC model based on the slip-spring framework is proposed to understand the linear rheology of WLMs. Specifically, the dynamics of important relaxation mechanisms such as reptation, constraint release, and dynamic union-scission in WLMs was simulated as separate kMC events. The proposed methodology takes into consideration the important relaxation mechanism of constraint release, which has not been considered in the existing studies [9,10,15,41]. Furthermore, all these studies considered the mean-field assumption to model the kinetics of union-scission in WLMs. This assumption is eliminated in the proposed kMC framework by modeling the living nature of WLMs with both

the mean-field and the diffusion-controlled kinetic regimes. Since this mesoscopic model considers important relaxation mechanisms, it can be used to analyze the interaction among different mechanisms that contribute to the viscoelastic properties of self-assembled micellar structures like wormlike micelles.

For demonstration purposes, the proposed framework was employed to study the viscoelastic properties of WLMs in a solution of sodium oleate and sodium chloride. Subsequently, this model was used to predict the loss and storage modulus of the WLMs. It was observed that the model predictions were in good agreement with the experimental data [39] and the existing theory of WLM relaxation [11,34,37]. Moreover, the length of WLMs predicted from a thermodynamic model was incorporated into the rheology model to capture the variation of WLM relaxation time with changing salt concentration and pH. Utilizing the relaxation time, the zero-shear viscosity was calculated, and the effect of salt concentration and pH on the zero shear viscosity was explained by the proposed framework. The fall in zero shear viscosity and its gradient due to increasing salt concentration and pH was attributed to the living nature of the WLMs. Specifically, it was inferred that at a high counterion concentration resulting from a high salt concentration or pH, the reptation and union-scission mechanisms have opposing effects on zero-shear viscosity. This explained the observed sensitivity of the zero shear viscosity of solution with the salt concentration and pH.

As a future study, this framework can be extended in a simple fashion to model the nonlinear rheology of the WLMs by altering the periodic boundary conditions used in this work. Another interesting direction can be utilizing the proposed methodology to study other nonlinear viscoelastic phenomenon such as stress-induced breakage of WLMs in solution. Also, including the crucial physics such as bending of WLM segments to study the cross-over mechanism of various WLM solutions, which explains tight entanglement regimes in WLMs, can be an important contribution to this field.

#### CRediT authorship contribution statement

**Silabrata Pahari:** Methodology, Software, Formal analysis, Writing – original draft. **Bhavana Bhadriraju:** Validation, Investigation, Resources, Writing – review & editing. **Mustafa Akbulut:** Conceptualization, Writing – review & editing. **Joseph Sang-II Kwon:** Conceptualization, Validation, Writing – review & editing, Supervision, Project administration.

#### Declaration of Competing Interest

The authors declare that they have no known competing financial interests or personal relationships that could have appeared to influence the work reported in this paper.

#### Acknowledgments

The authors gratefully acknowledge financial support from the National Science Foundation (CBET-1804407), the Department of Energy (DE-FE0031778, DE-EE0007888-10-8), the Texas A&M Energy Institute, the Artie McFerrin Department of Chemical Engineering, and the Texas A&M High Performance Research Computing facility.

#### Appendix A. Supplementary material

Supplementary data associated with this article can be found, in the online version, at <https://doi.org/10.1016/j.jcis.2021.05.032>.

#### References

- [1] X. Pei, J. Zhao, Y. Ye, Y. You, X. Wei, Wormlike micelles and gels reinforced by hydrogen bonding in aqueous cationic gemini surfactant systems, *Soft Matter* 7 (6) (2011) 2953–2960.
- [2] A. Bhadani, M. Tani, T. Endo, K. Sakai, M. Abe, H. Sakai, New ester based gemini surfactants: the effect of different cationic headgroups on micellization properties and viscosity of aqueous micellar solution, *PCCP* 17 (29) (2015) 19474–19483.
- [3] T.A. Camesano, R. Nagarajan, Micelle formation and cmc of gemini surfactants: a thermodynamic model, *Colloids Surf. A* 167 (1–2) (2000) 165–177.
- [4] C.A. Dreiss, Wormlike micelles: where do we stand? recent developments, linear rheology and scattering techniques, *Soft Matter* 3 (8) (2007) 956–970.
- [5] S.R. Raghavan, E.W. Kaler, Highly viscoelastic wormlike micellar solutions formed by cationic surfactants with long unsaturated tails, *Langmuir* 17 (2) (2001) 300–306.
- [6] S.R. Raghavan, J.F. Douglas, The conundrum of gel formation by molecular nanofibers, wormlike micelles, and filamentous proteins: gelation without cross-links?, *Soft Matter* 8 (33) (2012) 8539–8546.
- [7] J. Yang, Viscoelastic wormlike micelles and their applications, *Current Opin. Colloid Interface Sci.* 7 (5–6) (2002) 276–281.
- [8] S. Pahari, P. Bhandakkar, M. Akbulut, J. Sang-II Kwon, Optimal pumping schedule with high-viscosity gel for uniform distribution of proppant in unconventional reservoirs, *Energy* (2020) 119231.
- [9] S. Candau, A. Khatory, F. Lequeux, F. Kern, Rheological behaviour of wormlike micelles: effect of salt content, *Le J. de Phys.* IV 3 (C1) (1993) C1–197.
- [10] M.E. Cates, S.M. Fielding, Rheology of giant micelles, *Adv. Phys.* 55 (7–8) (2006) 799–879.
- [11] M. Cates, Reptation of living polymers: dynamics of entangled polymers in the presence of reversible chain-scission reactions, *Macromolecules* 20 (9) (1987) 2289–2296.
- [12] M. Doi, S.F. Edwards, S.F. Edwards, *The theory of Polymer Dynamics*, Oxford University Press, 1988, p. 73.
- [13] F. Lequeux, Reptation of connected wormlike micelles, *EPL (Europhysics Letters)* 19 (8) (1992) 675.
- [14] P.V.D. Shoot, J.P. Wittmer, Linear aggregation revisited: Rods, rings and worms, *Macromol. Theory Simul.* 8 (5) (1999) 428–432.
- [15] R.G. Larson, The lengths of thread-like micelles inferred from rheology, *J. Rheol.* 56 (6) (2012) 1363–1374.
- [16] S. Edwards, T.A. Vilgis, The tube model theory of rubber elasticity, *Rep. Prog. Phys.* 51 (2) (1988) 243.
- [17] P.-G. De Gennes, P.-G. Gennes, *Scaling Concepts in Polymer Physics*, Cornell University Press, 1979.
- [18] J.L. Viovy, M. Rubinstein, R.H. Colby, Constraint release in polymer melts: Tube reorganization versus tube dilation, *Macromolecules* 24 (12) (1991) 3587–3596.
- [19] S. Milner, T. McLeish, A. Likhman, Microscopic theory of convective constraint release, *J. Rheol.* 45 (2) (2001) 539–563.
- [20] R. Ball, M. Doi, S. Edwards, M. Warner, Elasticity of entangled networks, *Polymer* 22 (8) (1981) 1010–1018.
- [21] W.W. Graessley, D.S. Pearson, Stress-strain behavior in polymer networks containing nonlocalized junctions, *J. Chem. Phys.* 66 (8) (1977) 3363–3370.
- [22] C.C. Hua, J.D. Schieber, Segment connectivity, chain-length breathing, segmental stretch, and constraint release in reptation models. i. theory and single-step strain predictions, *J. Chem. Phys.* 109 (22) (1998) 10018–10027.
- [23] A.E. Likhman, Single-chain slip-link model of entangled polymers: Simultaneous description of neutron spin-echo, rheology, and diffusion, *Macromolecules* 38 (14) (2005) 6128–6139.
- [24] T. Uneyama, Y. Masubuchi, Multi-chain slip-spring model for entangled polymer dynamics, *J. Chem. Phys.* 137 (15) (2012) 154902.
- [25] Y. Masubuchi, H. Watanabe, G. Ianniruberto, F. Greco, G. Marrucci, Comparison among slip-link simulations of bidisperse linear polymer melts, *Macromolecules* 41 (21) (2008) 8275–8280.
- [26] M. Müller, K.C. Daoulas, Single-chain dynamics in a homogeneous melt and a lamellar microphase: A comparison between smart monte carlo dynamics, slithering-snake dynamics, and slip-link dynamics, *J. Chem. Phys.* 129 (16) (2008) 164906.
- [27] V.C. Chappa, D.C. Morse, A. Zippelius, M. Müller, Translationally invariant slip-spring model for entangled polymer dynamics, *Phys. Rev. Lett.* 109 (14) (2012) 148302.
- [28] G.G. Vogiatzis, G. Megariotis, D.N. Theodorou, Equation of state based slip spring model for entangled polymer dynamics, *Macromolecules* 50 (7) (2017) 3004–3029.
- [29] K.D. Danov, P.A. Kralchevsky, R.D. Stanimirova, S.D. Stoyanov, J.L. Cook, I.P. Stott, Analytical modeling of micelle growth. 4. molecular thermodynamics of wormlike micelles from ionic surfactants: Theory vs. experiment, *J. Colloid Interface Sci.* 584 (2020) 561–581.
- [30] K.D. Danov, P.A. Kralchevsky, S.D. Stoyanov, J.L. Cook, I.P. Stott, Analytical modeling of micelle growth. 2. molecular thermodynamics of mixed aggregates and scission energy in wormlike micelles, *J. Colloid Interface Sci.* 551 (2019) 227–241.
- [31] I.C. Sanchez, R.H. Lacombe, An elementary molecular theory of classical fluids. pure fluids, *J. Phys. Chem.* 80 (21) (1976) 2352–2362.
- [32] W. Van Gunsteren, H.J. Berendsen, Algorithms for macromolecular dynamics and constraint dynamics, *Mol. Phys.* 34 (5) (1977) 1311–1327.

- [33] M.N. Rosenbluth, A.W. Rosenbluth, Monte carlo calculation of the average extension of molecular chains, *J. Chem. Phys.* 23 (2) (1955) 356–359.
- [34] B. O'Shaughnessy, J. Yu, Rheology of wormlike micelles: two universality classes, *Phys. Rev. Lett.* 74 (21) (1995) 4329.
- [35] G.G. Vogiatis, E. Vogiatis, D.N. Theodorou, Monte carlo simulations of a coarse grained model for an athermal all-polystyrene nanocomposite system, *Eur. Polymer J.* 47 (4) (2011) 699–712.
- [36] W. Zou, R.G. Larson, A mesoscopic simulation method for predicting the rheology of semi-dilute wormlike micellar solutions, *J. Rheol.* 58 (3) (2014) 681–721.
- [37] J. Padding, E. Boek, Evidence for diffusion-controlled recombination kinetics in model wormlike micelles, *EPL (Europhysics Letters)* 66 (5) (2004) 756.
- [38] W. Carl, R. Makhloifi, M. Kröger, On the shape and rheology of linear micelles in dilute solutions, *J. Phys. II* 7 (6) (1997) 931–946.
- [39] H. Lu, Q. Shi, Z. Huang, ph-responsive anionic wormlike micelle based on sodium oleate induced by nacl, *J. Phys. Chem. B* 118 (43) (2014) 12511–12517.
- [40] T. Hayat, S. Nadeem, S. Asghar, Periodic unidirectional flows of a viscoelastic fluid with the fractional maxwell model, *Appl. Math. Comput.* 151 (1) (2004) 153–161.
- [41] M. Grmela, F. Chinesta, A. Ammar, Mesoscopic tube model of fluids composed of worm-like micelles, *Rheologica acta* 49 (5) (2010) 495–506.
- [42] Niranjan Sitapure, Robert Epps, Milad Abolhasani, Joseph Sang-II Kwon, Multiscale modeling and optimal operation of millifluidic synthesis of perovskite quantum dots: Towards size-controlled continuous manufacturing, *Chemical Engineering Journal* 413 (2021) 127905.
- [43] Niranjan Sitapure, Tian Qiao, Dong Hee Son, Joseph Sang-II Kwon, Kinetic Monte Carlo modeling of the equilibrium-based size control of CsPbBr<sub>3</sub> perovskite quantum dots in strongly confined regime, *Computers and Chemical Engineers* 139 (2020) 106872.
- [44] Hyun-Kyu Choi, Joseph Sang-II Kwon, Multiscale modeling and control of Kappa number and porosity in a batch-type pulp digester, *AIChE Journal* 65 (6) (2019).
- [45] Joseph Sang-II Kwon, Michael Nayhouse, Panagiotis D. Christofides, Gerasimos Orkoulas, Modeling and control of crystal shape in continuous protein crystallization, *Chemical Engineering Science* 107 (2014) 47–57.
- [46] Marquis Crose, Joseph Sang-II Kwon, Michael Nayhouse, Dong Ni, Panagiotis D. Christofides, Multiscale modeling and operation of PECVD of thin film solar cells, *Chemical Engineering Science* 136 (2015) 50–61.
- [47] Dongheon Lee, Alec Mohr, Joseph Sang-II Kwon, Hung-Jen Wu, Kinetic Monte Carlo modeling of multivalent binding of CTB proteins with GM1 receptors, *Computers & Chemical Engineering* 118 (2018) 283–295.